Rashba split surface states in BiTeBr

2013 New J. Phys. 15 075015

(http://iopscience.iop.org/1367-2630/15/7/075015)

New Journal of Physics
The open access journal for physics

Rashba split surface states in BiTeBr

S V Eremeev[1,2], I P Rusinov[2], I A Nechaev[2,3] and E V Chulkov[3,4,5]

[1] Institute of Strength Physics and Materials Science, 634021 Tomsk, Russia
[2] Tomsk State University, 634050 Tomsk, Russia
[3] Donostia International Physics Center (DIPC), E-20018 San Sebastián/Donostia, Basque Country, Spain
[4] Departamento de Física de Materiales and Centro Mixto CSIC-UPV/EHU, Facultad de Ciencias Químicas, Universidad del Pais Vasco/Euskal Herriko Unibertsitatea, Apartado 1072, E-20080 San Sebastián/Donostia, Basque Country, Spain
E-mail: waptctce@ehu.es

New Journal of Physics **15** (2013) 075015 (13pp)
Received 23 January 2013
Published 17 July 2013
Online at http://www.njp.org/
doi:10.1088/1367-2630/15/7/075015

Abstract. Within density functional theory, we study the bulk band structure and surface states of BiTeBr. We consider both ordered and disordered phases, which differ in atomic order in the Te–Br sublattice. On the basis of relativistic *ab initio* calculations, we show that the ordered BiTeBr is energetically preferable as compared with the disordered one. We demonstrate that both Te- and Br-terminated surfaces of the ordered BiTeBr hold surface states with a giant spin–orbit splitting. The Te-terminated surface-state spin splitting has Rashba-type behavior with the coupling parameter $\alpha_R \sim 2\,\mathrm{eV\AA}$.

[5] Author to whom any correspondence should be addressed.

Contents

1. Introduction

Nowadays, a controllable manipulation of the electronic spin degree-of-freedom without recourse to an external magnetic field is a process in technological demand, since it constitutes the basis of functionality of spintronics devices [1]. An obvious candidate for the phenomenon underlying this process is spin–orbit interaction (SOI) that couples the spin and momentum of electrons. In the case of two-dimensional (2D) geometries (surfaces, asymmetric quantum wells, etc), the SOI may result in a spin splitting of electron states, which has the nature of the so-called Rashba effect [2]. This splitting can be tuned by an applied electric field [3–7], which opens up a pathway for realizing electric-field spin manipulation. There are two key operating characteristics here: the Rashba energy, E_R, and the momentum offset of split states, k_R, which together define the Rashba coupling strength as $\alpha_R = 2E_R/k_R$.

In the conventional semiconductor structures, where the Rashba effect has been revealed for the first time, the parameter α_R is of the order of 10^{-1} eV Å (see e.g. [4, 8, 9]). However, for room-temperature applications of spintronics devices, it is crucial to have α_R as large as possible. As a result, over a long period of time the Rashba effect has been attracting great interest, and many systems with a large Rashba spin splitting have been discovered. It was found that the $\bar{\Gamma}$ surface state on Au(111) has a Rashba splitting with α_R that is about five times larger than that in the semiconductor heterostructures (see e.g. [10–12] and the detailed discussion in [13]). A significantly larger α_R has been reported for a surface state at the Bi surfaces [14]. In seeking a way to tune spin–orbit splitting of surface states, it was shown that, for instance, in the case of the Au(111) surface it can be done with deposition of Ag atoms [15, 16]. As was demonstrated in [17–23], a more efficient way to modify spin splitting of surface states is surface alloying of heavy elements (Bi, Pb, Sb) on noble-metal surfaces. In this case, one arrives at a Rashba-type split surface state with α_R that is about one order of magnitude greater than that in the semiconductor structures.

To go further in the possible tuning of spin–orbit splitting of electron states, quantum-well states evolving by the confinement of electrons in ultrathin metal films have been considered. In the presence of both the surface and the interface with a substrate, the number of impacts on the splitting doubles. As was reported, e.g., in [24], a Bi monolayer film on Cu(111) can provide with spin–orbit split quantum-well states in the unoccupied electronic structure, which are characterized by α_R similar to that in the surface alloys. However, apart from a large spin–orbit splitting, for an efficient spintronics application in the way specified above, a semiconductor substrate and the absence of spin-degenerate carriers in quite a wide energy interval are more promising.

In the case of a semiconductor substrate (e.g. ultrathin Pb films on Si(111) [25]), quantum well states show a Rashba splitting as small as in the semiconductor structures. A large Rashba spin splitting on a semiconductor substrate can be reached, for example, by means of a Bi-trimer adlayer on a Si(111) surface (see also [26]), where the splitting has a similar origin as in the Bi/Ag(111) surface alloy and a close value for the parameter α_R [27]. Nevertheless, the found spin-split 2D states cannot be described well by a simple Rashba model, where a parabolic dispersion with a positive effective mass combines with the spin splitting that is linear in electron momentum. This motivates an active search for new materials and a revision of the already known systems with an SOI that under certain conditions can lead to a technologically meaningful spin splitting of a free-electron-like state at a semiconductor surface. In that sense, the reexamining of bismuth tellurohalides, where a Rashba-type spin splitting of states has been revealed to be caused by intrinsic inversion asymmetry of bulk crystal potential [28–33], can be considered as a great advance made recently in the search. Actually, it was shown that Te-terminated surfaces of BiTeCl and BiTeI possess a giant spin–orbit splitting of a free-electron-like surface state [30–33].

The mentioned bismuth tellurohalides have hexagonal crystal structures [34] and are characterized by ionic bonding with large charge transfer from Bi to halide- and Te-atomic layers. The crystal structure is made up of alternating hexagonal layers Te–Bi–I(Cl) stacked along the hexagonal axis. Besides, each three-layer group Te–Bi–I(Cl) forms a TL block, and the distance between the blocks is about one and a half times greater than the interlayer distances within the Te–Bi–I(Cl) TL structure. Such a three-layered structure breaks the inversion symmetry of bulk crystal potential, which leads to appearance of the Rashba-type spin–orbit splitting of the bulk bands [28, 30]. Due to the layered crystal structure, the bismuth tellurohalide surfaces can be terminated by a Te- or halide-atom layer. Both these terminations hold spin-split surface states [30–33]. These states emerge by splitting off either from the lowest conduction band (for the Te termination) or from the uppermost valence band (for the halide-atom termination). The splitting off is caused by changes in potential (decreasing at the Te-terminated surface and increasing at the halide-atom-terminated surface) within the near-surface layers [30] as compared with the bulk region, which is a consequence of the strong ionicity.

In addition to BiTeCl and BiTeI, the bismuth–tellurohalide group is known to have one more semiconductor—BiTeBr. It was previously reported [34, 35] that its layered crystal structure is a disordered centrosymmetric one, where tellurium and bromine atoms are randomly distributed within two layers adjacent to a Bi-atomic layer [34, 35]. As a consequence, both the bulk and surface electronic structure of the disordered BiTeBr were never addressed before, while the Rashba-type splitting of the bulk bands in the ordered non-centrosymmetric phase of BiTeBr was predicted [30]. The spin splitting has been found to be larger than that in BiTeCl and smaller than that in BiTeI.

Recently, it has been reported that a single-crystalline BiTeBr was grown by the chemical vapor transport method, and by x-ray diffraction measurements its ordered structure was confirmed [36]. Moreover, angle-resolved photoemission spectroscopy (ARPES) measurements of the ordered BiTeBr demonstrated a series of Rashba-type split states localized in the near-surface region. These states were interpreted in a similar way as in [28], where the spin-split state experimentally observed in BiTeI has been considered as quantized subbands of the bulk conduction band. However, the latter was questioned in [31, 32], where the existence of the aforementioned surface state at the Te-terminated surface of BiTeI has been experimentally corroborated. Additionally, certain doubts are raised regarding the fact that in [36] the

band bending potential was obtained within the Poisson–Shrödinger method, assuming static dielectric constants which are quite different from its available experimental [37] and calculated [38] values. The smooth band bending potential was used in the model that does not reflect the layered structure of this material. Probably, this can explain wrong values of ε used to describe the band bending. Finally, the spin texture of the states experimentally observed in BiTeBr remains to be examined both theoretically and experimentally.

In this paper, we examine both disordered and ordered phases of BiTeBr. We model the crystal structure of the ordered phase as that of BiTeI but with Br instead of I and the lattice parameters were taken from [34]. Atomic positions are obtained within a structural optimization. On the basis of *ab initio* calculations, we show that the ordered structure is energetically preferable that agrees well with experiment [36]. We demonstrate that both the Te- and Br-terminated surfaces of the ordered BiTeBr hold the spin–orbit split surface states emerged by splitting off from the bulk conduction or valence band like in other bismuth tellurohalides. For the practical use, as in the case of BiTeCl and BiTeI the Te-terminated surface of BiTeBr is more suitable than the halide-atom-terminated one, since it holds a surface state that has a free-electron-like dispersion and a large Rashba-type spin splitting. At the same time, BiTeBr has an advantage over BiTeCl and BiTeI. As compared with BiTeCl, the ordered bromide has a larger Rashba spin splitting of the Te-terminated surface state and a wider bulk band gap. In contrast to BiTeI, the surface state is larger split off from the bulk conduction band and more isotropic. We also ascertain that apart from the revealed surface state localized within the topmost TL of the ordered BiTeBr, there appear additional states which lie predominantly in the projected bulk band continuum and are localized, respectively, in the second and third TLs. The resulting surface-electronic structure reproduces well the experimental observation. By examining the spin texture of the Br- and Te-terminated surface states, we show that the Rashba-type coupling of the in-plane spin component with the electron momentum and negligibly small out-of-plane spin component is characteristic of the Te-terminated surface state only and is merely within the bulk band-gap energy region.

2. The computational method

The structural optimization and electronic band calculations are performed within the density functional formalism as implemented in VASP [39, 40]. We use the all-electron projector augmented wave (PAW) [41, 42] basis sets with the generalized gradient approximation (GGA) of Perdew, Burke and Ernzerhof (PBE) [43] to the exchange correlation potential. The Hamiltonian contains the scalar relativistic corrections, and the SOI was taken into account by the second variation method [44]. The energy cutoff for the plane wave expansion was set to 11.5 Ha and a k-point mesh of $7 \times 7 \times 7$ was used for the bulk calculation. The total-energy convergence was better than 1.0×10^{-7} Ha. The atomic positions were obtained during a relaxation procedure at fixed volume until forces became less than 1.0×10^{-5} Ha Bohr^{-1}.

To treat the bulk disordered phase effect, we employ two approaches. The first one is a supercell approach used within VASP, where a $4 \times 4 \times 1$ supercell with several configurations for randomly distributed Te and Br atoms were considered. The second approach is virtual crystal approximation (VCA) as implemented in the ABINIT code [45], where the configuration averaged potential of a gray atom occupying a site in the Te–Br sublattice is defined as a mixture $V_{\mathrm{VCA}} = xV_{\mathrm{Br}} + (1-x)V_{\mathrm{Te}}$ of Br (V_{Br}) and Te (V_{Te}) pseudopotentials with $x = 0.5$. We used GGA-PBE Hartwigsen–Goedecker–Hutter

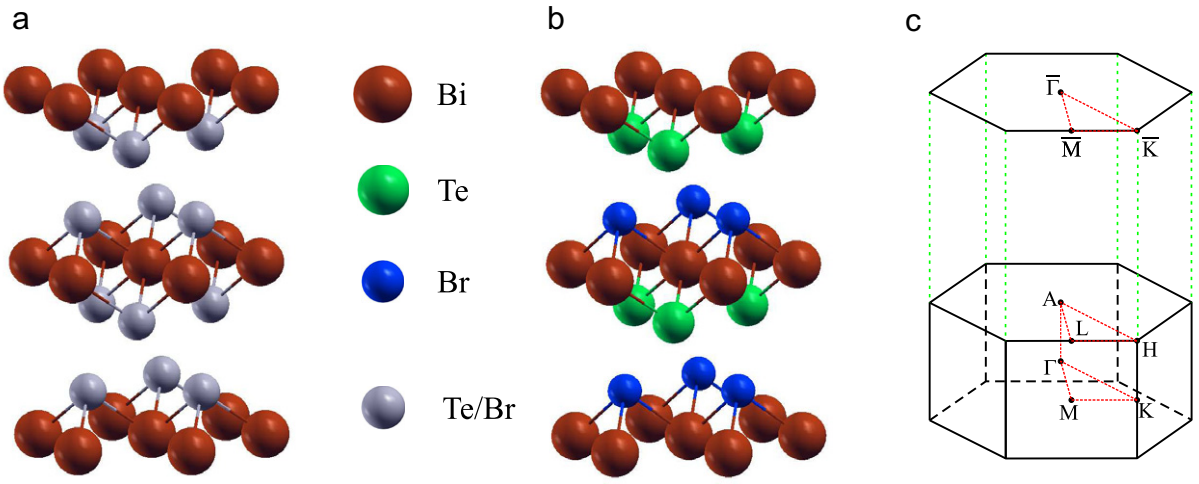

Figure 1. Atomic structure of BiTeBr: (a) disordered structure with lattice parameters and atomic positions taken from [34] and (b) optimized ordered structure. (c) The bulk Brillouin zone (bottom) and projected onto the (0001) plane 2D Brillouin zone (top).

(HGH) [46] relativistic norm-conserving pseudopotentials taken from http://cvs.berlios.de/cgi-bin/viewvc.cgi/cp2k/potentials/Goedecker/abinit/pbe/ which include the SOI. In the VCA calculations, atoms occupied the positions reported in [34]. To find the total-energy gain or loss caused by atomic ordering, the band structure of the ordered BiTeBr has been also calculated with the use of ABINIT and the VASP-derived relaxed atomic positions. All these ABINIT calculations were performed with $7 \times 7 \times 7$ **k**-point sampling of the bulk Brillouin zone, the plane-wave energy cutoff of 20 Ha and the total-energy convergence criterion of 1.0×10^{-12} Ha.

The surface of the ordered BiTeBr formed under cleavage can have Te-layer or Br-layer termination. To simulate semi-infinite BiTeBr(0001), using VASP we consider a 24 atomic layer slab with the bromine side (for the Te-terminated surface) or tellurium side (for the Br-terminated surface) passivated by hydrogen monolayer. A vacuum spacer of 20 Å was included to ensure negligible interaction between neighboring slabs. The k-point mesh of $9 \times 9 \times 1$ was used for the Brillouin zone of the surface unit cell. The slab geometry was initially derived from the aforementioned relaxed bulk crystal structure and further corrected by structure optimization of the topmost TLs until the forces that affected them became less than 1.0×10^{-4} Ha Bohr^{-1}.

3. Calculation results and discussion

In earlier works [34, 35], the CdI_2 hexagonal structure for BiTeBr was reported. This structure differs from that of BiTeI in that Br and Te atoms are statistically distributed over I_2-type sites (figure 1(a)). According to [34], the mixed Te/Br layers are located at a distance of ± 1.806 Å from the central Bi layer. To study the geometry of the disordered phase, we constructed a set of $4 \times 4 \times 1$ supercells with different configurations of randomly distributed Te and Br atoms. The simulation shows that, owing to markedly different charge transfer from the Bi atom to Br and Te atoms, the Bi layer acquires a substantial rippling of ~0.7 Å. This value is larger than the rippling within the Te/Br layer, which amounts to ~0.4 Å. Such a huge corrugation of atomic layers leads to remarkable variation (from 1.3 to 2 Å) of the distance

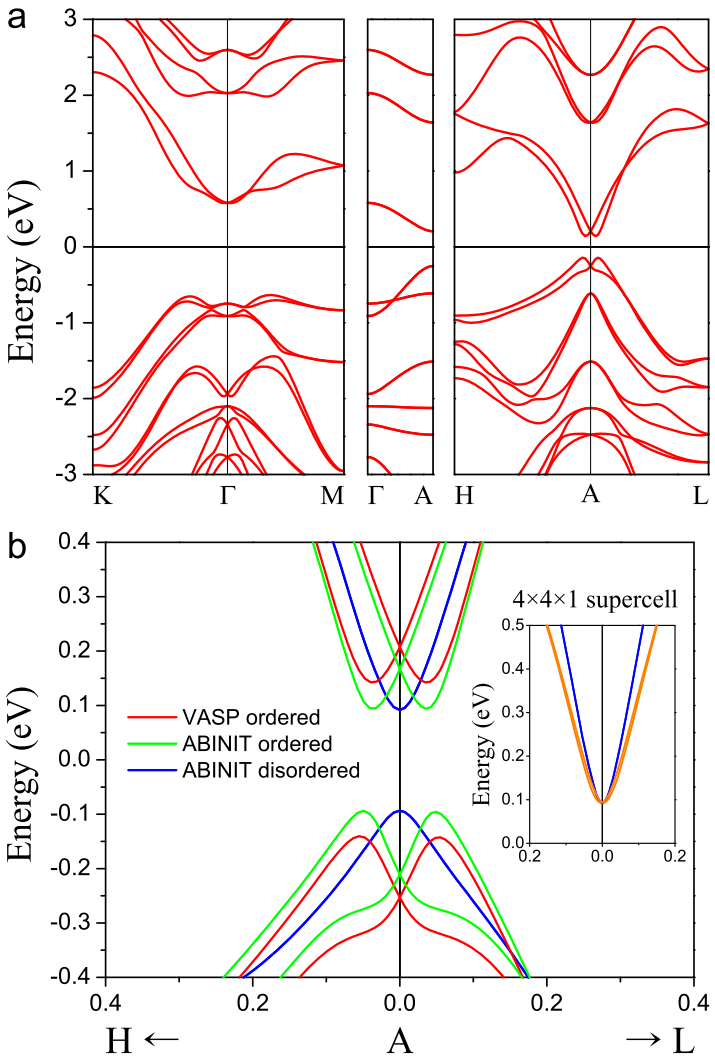

Figure 2. (a) Band structure calculated by the VASP along high-symmetry directions of the Brillouin zone for the BiTeBr ordered phase and (b) magnified view of the bulk electronic structure in the vicinity of the A point calculated with the use of both the PAW (VASP) and pseudopotential (ABINIT) approaches; the inset in panel (b) shows the lowest conduction band in the vicinity of the A point calculated within the $4 \times 4 \times 1$ supercell (orange line) and within the VCA (blue line).

between Bi atoms of the central rippled layer and atoms of the adjacent Te/Br layer. As a consequence, the resulting atomic structure differs essentially from that predicted in [34]. Next we considered the BiTeI-type ordered structure (figure 1(b)). In this system, interlayer distances obtained within the structural optimization are 1.769 Å between Bi and Te layers and 1.917 Å between Bi and Br layers. The ordered BiTeBr gains an energy of ∼180 meV per formula unit with respect to the disordered supercells. The VCA calculation confirms the preference of the ordered phase.

In figure 2(a), we show the bulk band structure calculated by the VASP code for the ordered BiTeBr. As clearly seen in the figure, both the conduction band minimum (CBM) and the

Table 1. Rashba coupling parameters α_R (eVÅ) for the bulk valence and conduction bands in the vicinity of the A point in the *A–H* and *A–L* directions. The calculated values for the bulk band gap, E_g, are also presented.

		Valence band		Conduction band	
	E_g (meV)	*A–H*	*A–L*	*A–H*	*A–L*
VASP	283	4.33	4.36	3.52	3.57
ABINIT	187	4.72	4.93	3.97	4.06

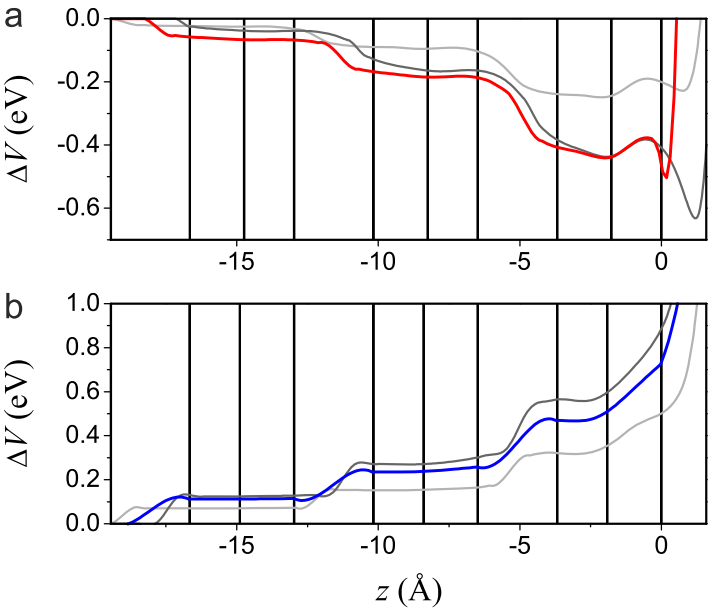

Figure 3. The change of the potential in the near-surface layers of the crystal with respect to that in the central, bulk-like layers: (a) Te-terminated surface (red line) and (b) Br-terminated surface (blue line). $z = 0$ corresponds to the topmost atomic layer. Dark and light gray lines show ΔV for BiTeCl and BiTeI taken from [30] and [33], respectively.

valence band maximum (VBM) demonstrate a giant Rashba-type spin splitting in the *H–A–L* plane. This spin splitting is characterized by a slightly anisotropic momentum offset k_R that in the *A–H* and *A–L* directions is ∼0.05 and 0.04 Å^{-1} for the VBM and CBM, respectively. The Rashba energy for the VBM is approximately twice that for the CBM (111 meV versus 66 meV). As a result, it provides a noticeably larger spin–orbit coupling for the upper valence-band states as compared with the lower conduction-band states (see table 1).

As seen in figure 2(b), the pseudopotential ABINIT calculations performed for the ordered BiTeBr confirm the large spin–orbit splitting in the vicinity of the A point. Moreover, we have obtained values for the Rashba parameters which are very close to those found with VASP (see α_R in table 1). The bulk band gap evaluated by ABINIT is about 100 meV smaller than that obtained from the VASP calculations. The spectrum calculated within the VCA for the disordered phase shows practically the same band gap and demonstrates the expected lack of

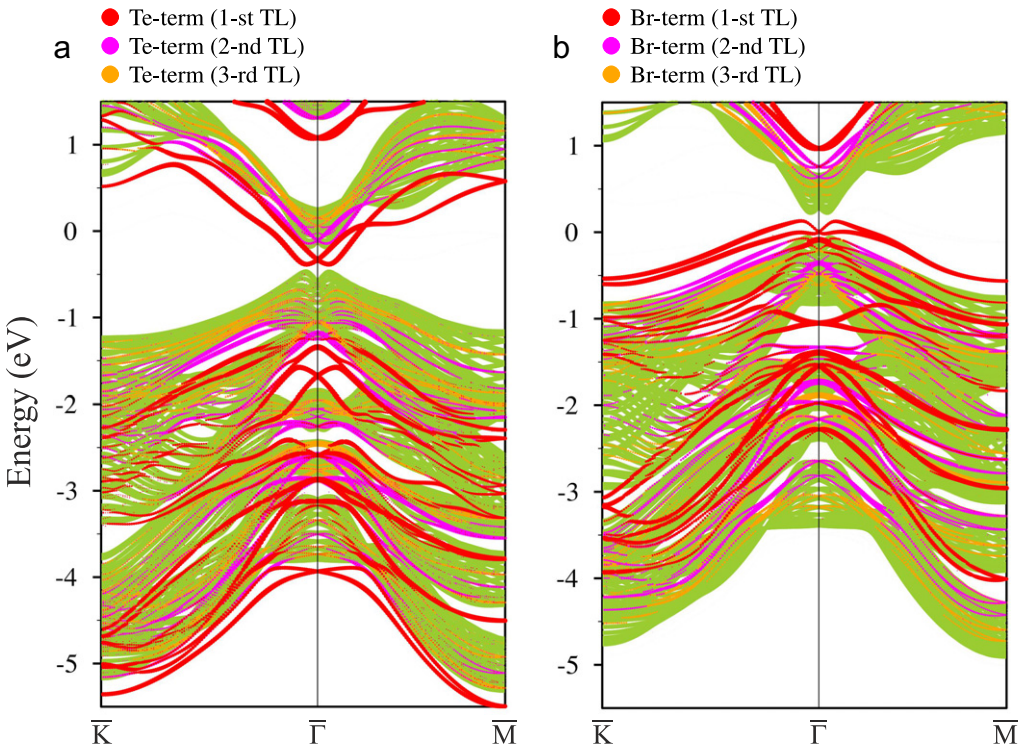

Figure 4. Electronic structure of a BiTeBr(0001) slab: (a) Te-terminated surface and (b) Br-terminated surface. The red, pink and orange circles denote weights of the states localized in the first, second and third TLs of the surface under consideration; light gray circles mark the states localized on the H-terminated side of the slab. The projected bulk band structure is shown in green.

spin splitting of the bulk bands due to the presence of inversion symmetry in the disordered structure. Note that the spin splitting of the bulk bands obtained within the supercell approach is negligible, and it agrees well with the VCA result (figure 2(b), inset), which indicates that the chosen $4 \times 4 \times 1$ geometry is well suited for describing the disordered BiTeBr.

As was mentioned above, the spin-split surface states of BiTeI and BiTeCl emerge as a result of splitting off from the lowest conduction band (at the Te-terminated surface) or from the uppermost valence band (at the halide-atom-terminated surface). The splitting off is caused by the potential change, ΔV, in the near-surface layers of the crystal with respect to that in central, bulk-like layers. Such a potential change is negative at the Te-terminated surface and positive at the Cl(I) atom-terminated surface [30, 33]. In both cases, ΔV bears a stepwise character owing to a clearly defined three-layered structure of bismuth tellurohalides. A similar behavior of ΔV occurs on the surfaces of the ordered BiTeBr, as seen in figure 3, where the change of the potential within the three outermost TLs on both surface terminations is shown. As one can see at the Te-terminated surface the potential bending is two times larger with respect to that in BiTeI and is comparable with that in BiTeCl. The latter indicates that the Te-terminated surface of BiTeBr should hold the surface state well separated from the bulk band edge similarly as it is in chloride. At the Br-terminated surface the potential bending has an intermediate value between other bismuth tellurohalides. Such a dependence of ΔV on X element in BiTeX series ($X =$ Cl, Br, I) is related to the peculiarities of the charge redistribution in bulk BiTeX where

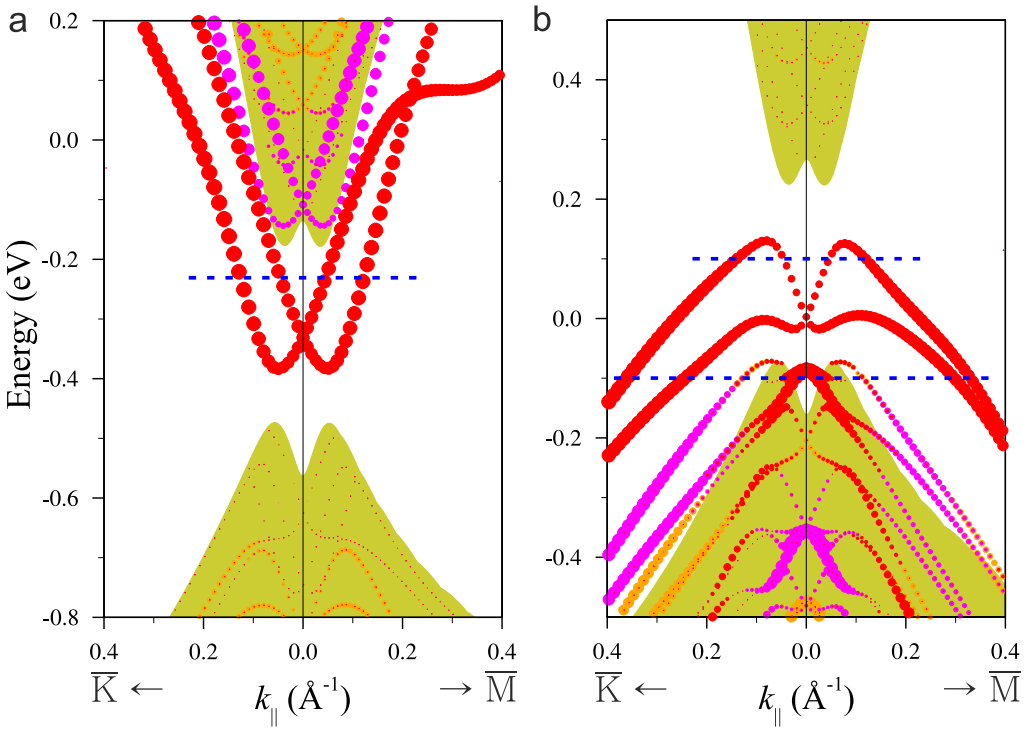

Figure 5. Magnified view of the electronic structure of Te-terminated (a) and Br-terminated (b) BiTeBr(0001) surfaces in the vicinity of $\bar{\Gamma}$ (colors correspond to those marked in figure 4).

the charge transfer from Bi to *X* decreases in the sequence Cl–Br–I. At the same time Te atom charge is practically equal in BiTeCl and BiTeBr, being smaller than that in BiTeI.

The negative ΔV observed at the Te-terminated surface of the ordered BiTeBr leads to a downward shift of energies of the electron states trapped in the stepwise surface potential (figure 4(a)). These states are predominantly localized in the first three TLs. At the Br-terminated surface, an upward shift of energies of the trapped states is provided by the positive ΔV (figure 4(b)). As a net result, for both terminations the changes of the electronic structure of BiTeBr under the surface formation lead to the emergence of the spin-split surface states in the bulk band gap (figure 5). Other trapped states are also offset in momentum, reflecting a large spin–orbit splitting. They appear to be partially overlapping the valence band continuum except the local energy-gap regions within bulk continuum states where the trapped states should be well resolved in ARPES at high binding energies.

At the Te-terminated surface (figure 5(a)), the spin–orbit split surface state localized in the topmost TL replicates the conduction band edge. The degeneracy point of the surface spin-split state is 150 meV lower than the CBM. Within the energy gap region, the surface-state dispersion demonstrates the free-electron-like parabolic character. The spin splitting of the state in the $\bar{\Gamma}$–$\bar{K}$ ($\bar{\Gamma}$–$\bar{M}$) direction is characterized by $E_R = 0.052(0.051)$ eV and $k_R = 0.049(0.051)$ Å^{-1}, which yields $\alpha_R = 2.11(2.01)$ eVÅ. These values of the Rashba parameters fall in the error bar range of the respective experimental values reported in [36] for the first subband dispersion. It is worth emphasizing that the next split state generated by the staircase-like near-surface potential and lying right above the mentioned surface state is localized in the second TL and can be identified

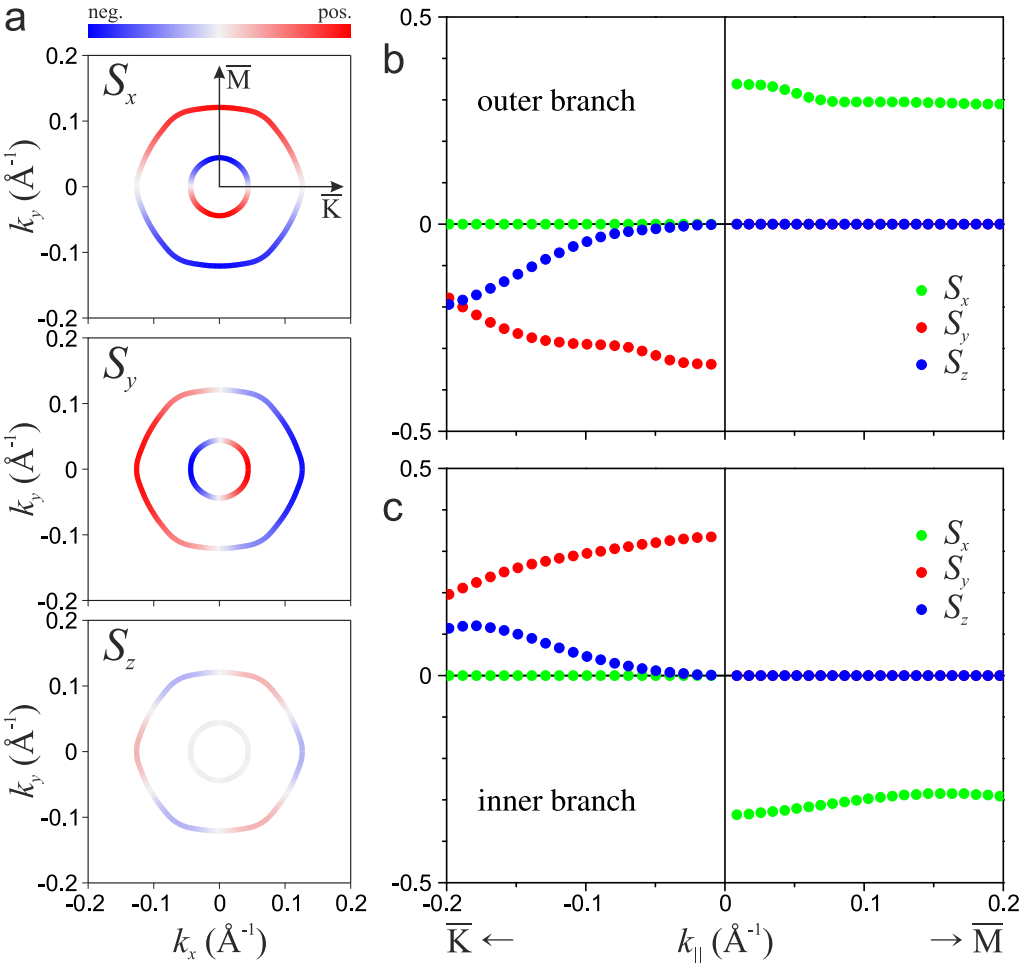

Figure 6. Spin structure of the spin-split surface states on the Te-terminated BiTeBr(0001) surface, as given by spin components S_x, S_y and S_z at an energy of 100 meV (see the horizontal dashed lines in figure 4) above the degeneracy point (a) and these spin components traced along the $\bar{\Gamma}$–$\bar{K}$ and $\bar{\Gamma}$–$\bar{M}$ directions for the outer (b) and inner (c) branches of the Rashba-split surface state. The z-axis coincides with the surface normal.

with the experimentally observed second subband. Actually, in the $\bar{\Gamma}$–$\bar{K}$ ($\bar{\Gamma}$–$\bar{M}$) direction the dispersion of this state is described by $E_R = 0.036(0.035)$ eV, $k_R = 0.040(0.043)$ Å^{-1} and $\alpha_R = 1.81(1.64)$ eVÅ, which are also in the error bar range of the experimental values of [36] for the second subband dispersion. As to the higher-lying trapped states, they are not clearly identified either theoretically or experimentally. By this comparison, we highlight that we have obtained the series of the 2D states which well reproduce the experimental observations.

The parabolic character of the Te-terminated surface state provides the circular shape of the constant energy contours (CEC) for the inner and outer branches of the spin-split surface state in the bulk band-gap region. As one can see in figure 6(a), in approaching the bulk conduction band the CEC for the outer branch acquires the hexagonal deformation that is already visible at 100 meV above the degeneracy point. The surface-state spin structure demonstrates counter-clockwise and clockwise in-plane helicity for the inner and outer branches, respectively, with

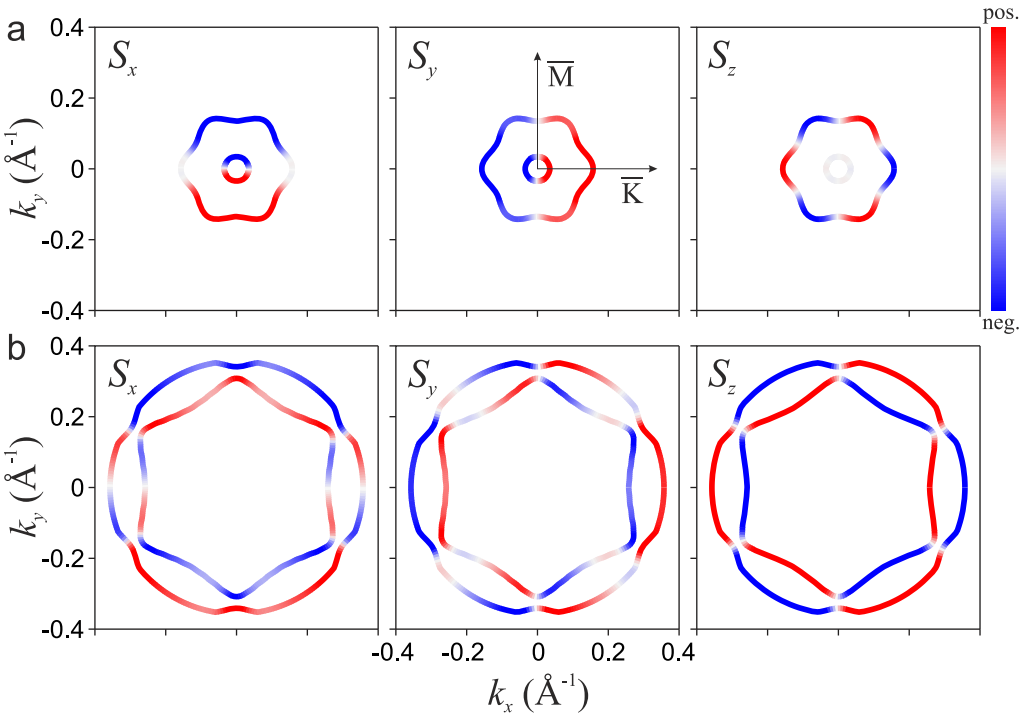

Figure 7. Spin structure of the spin-split surface states on the Br-terminated BiTeBr(0001) surface, as given by spin components S_x, S_y and S_z at an energy of 100 meV (see the horizontal lines in figure 4) above (a) and below (b) the degeneracy point. The z-axis coincides with the surface normal.

a small S_z spin component for both of them (figure 6(a)). Owing to symmetry constraints, the expectation value of the S_y and S_z spin components vanishes along $\bar{\Gamma}$–$\bar{\mathrm{M}}$, and they have maximal values along $\bar{\Gamma}$–$\bar{\mathrm{K}}$ at any chosen energy. In turn, S_x is zero along the $\bar{\Gamma}$–$\bar{\mathrm{K}}$ and reaches maximal values along the $\bar{\Gamma}$–$\bar{\mathrm{M}}$ direction. In figure 6(b), we show the absolute value of the Cartesian spin components as functions of $k_{||}$ for the inner and outer branches of the spin-split surface state. As one can see, for a small $k_{\bar{\mathrm{K}}}$ the $|S_z|$ component is negligibly small and, thus, the surface state is completely in-plane spin polarized. This component starts rising at $k_{\bar{\mathrm{K}}} > 0.1$ Å^{-1}, i.e. at an energy of 50 meV above the degeneracy point, which leads to a decrease of the in-plane spin components when approaching the bulk conduction states. Thus, owing to (i) the parabolic energy dispersion, (ii) the outermost TL localization and (iii) the in-plane helical spin structure within the band-gap energy region, the surface state on the Te-terminated surface of BiTeBr(0001) can be described as the Rashba-split surface state with a Rashba coupling parameter of ∼2 eV Å.

At the Br-terminated surface (figure 5(b)), the spin–orbit split surface state localized in the topmost TL lies entirely in the band gap right above the upper valence band and follows its edge. As one can see, the states localized in the second TL spread already along the valence-band edge in the $\bar{\Gamma}$–$\bar{\mathrm{K}}$ and $\bar{\Gamma}$–$\bar{\mathrm{M}}$ directions but they degenerate with bulk states in the close vicinity of $\bar{\Gamma}$. Furthermore, the second outermost-TL localized state arises at $\bar{\Gamma}$ in the valley of the valence band. The appearance of the second pair of the spin-split states in the gap and the second state at $\bar{\Gamma}$ is explained by the fact that the magnitude of the ΔV is larger than that on the Te-terminated surface (see figure 3). Such a ΔV provides a larger splitting off from the valence band edge.

In general features, the band-gap-lying outermost first TL-localized spin–orbit split surface state at the Br-terminated surface resembles those found at the halide-atom-terminated surface of BiTeCl and BiTeI [30, 33]. This state demonstrates noticeable anisotropy of the energy dispersion with respect to $k_{||}$, which results in the more complex shape of the CECs both above and below the degeneracy point (see figure 7). Such an anisotropic dispersion is accompanied by an appreciably out-of-plane spin polarization and entangled spin structure of the surface state, especially below the degeneracy point (figure 7).

Formally, the spin splitting of the Br-terminated surface state is characterized by $k_R = 0.079$ and $0.077\,\text{Å}^{-1}$ in the $\bar{\Gamma}$–$\bar{K}$ and $\bar{\Gamma}$–$\bar{M}$ directions, respectively, and by E_R equal to 130.2 meV ($\bar{\Gamma}$–$\bar{K}$) and 125.6 meV ($\bar{\Gamma}$–$\bar{M}$). These characteristics yield α_R equal to 3.29 and 3.26 eVÅ for the $\bar{\Gamma}$–$\bar{K}$ and $\bar{\Gamma}$–$\bar{M}$ directions, respectively. However, this spin-split surface state cannot be identified as the Rashba state owing to its dispersion and entangled spin structure.

4. Conclusions

Thus, we have investigated the atomic and electronic structures of BiTeBr. The total energy calculations of the ordered and disordered phases of BiTeBr have shown that the ordered structure is energetically preferable. We have found that the surfaces of the ordered BiTeBr hold surface states which demonstrate a giant spin–orbit spin splitting. These states emerge as a result of splitting off from the bulk conduction or valence band, owing to the potential bending within the near-surface layers, like in other bismuth tellurohalides, BiTeCl and BiTeI, studied earlier. The spin-split surface state at the Te-terminated surface, owing to its parabolic energy dispersion, outermost TL localization and in-plane helical spin structure preserved within the whole band-gap energy region, can be described as a Rashba-split surface state with the Rashba coupling parameter α_R of $\sim$2 eV Å, which is in good agreement with the recently reported experimental value of 2.0(7) eVÅ [36]. The Rashba-split state on Te-terminated BiTeBr has advantages over the other bismuth tellurohalides, which consist in the larger Rashba splitting and wider band gap as compared to BiTeCl and in the larger splitting off from the bulk conduction band with more isotropic energy dispersion within the band-gap region in comparison with BiTeI.

The band-gap surface state at the Br-terminated surface owing to its $k_{||}$ anisotropy and entangled spin structure cannot be identified as the Rashba-split state and thus has less appeal than the spin-split surface state at the Te-terminated surface.

Acknowledgments

We acknowledge partial support from the Basque Country Government, Departamento de Educación, Universidades e Investigación (grant no. IT-366-07) and the Spanish Ministerio de Ciencia e Innovación (grant no. FIS2010-19609-C02-00). Calculations were performed on the SKIF-Cyberia supercomputer of Tomsk State University.

References

[1] Žutić I, Fabian J and Das Sarma S 2004 *Rev. Mod. Phys.* **76** 323
[2] Rashba E I 1960 *Sov. Phys. Solid State* **2** 1109
Bychkov Y A and Rashba E I 1984 *JETP Lett.* **39** 78
Bychkov Y A and Rashba E I 1984 *J. Phys. C: Solid State Phys.* **17** 6039

[3] Datta S and Das B 1990 *Appl. Phys. Lett.* **56** 665
[4] Nitta J *et al* 1997 *Phys. Rev. Lett.* **78** 1335
[5] Grundler D 2000 *Phys. Rev. Lett.* **84** 6074
[6] Studer M *et al* 2009 *Phys. Rev. Lett.* **103** 027201
[7] Caviglia A D *et al* 2010 *Phys. Rev. Lett.* **104** 126803
[8] Lommer G, Malcher F and Rossler U 1988 *Phys. Rev. Lett.* **60** 728
[9] Luo J *et al* 1990 *Phys. Rev.* B **41** 7685
[10] LaShell S, McDougall B A and Jensen E 1996 *Phys. Rev. Lett.* **77** 3419
[11] Nicolay G *et al* 2001 *Phys. Rev.* B **65** 033407
[12] Hoesch M *et al* 2004 *Phys. Rev.* B **69** 241401
[13] Bihlmayer G *et al* 2006 *Surf. Sci.* **600** 3888
[14] Koroteev Yu M *et al* 2004 *Phys. Rev. Lett.* **93** 046403
[15] Cercellier H *et al* 2004 *Phys. Rev.* B **70** 193412
[16] Popović D *et al* 2005 *Phys. Rev.* B **72** 045419
[17] Nakagawa T *et al* 2007 *Phys. Rev.* B **75** 155409
[18] Ast C R *et al* 2007 *Phys. Rev. Lett.* **98** 186807
[19] Bihlmayer G, Blügel S and Chulkov E V 2007 *Phys. Rev.* B **75** 195414
[20] Ast C R *et al* 2008 *Phys. Rev.* B **77** 081407
[21] Mirhosseini H *et al* 2009 *Phys. Rev.* B **79** 245428
[22] Bentmann H *et al* 2011 *Phys. Rev.* B **84** 115426
[23] Gierz I *et al* 2010 *Phys. Rev.* B **81** 245430
[24] Mathias S *et al* 2010 *Phys. Rev. Lett.* **104** 066802
[25] Dil J H *et al* 2008 *Phys. Rev. Lett.* **101** 266802
[26] Yaji K *et al* 2010 *Nature Commun.* **1** 17
[27] Gierz I *et al* 2009 *Phys. Rev. Lett.* **103** 046803
[28] Ishizaka K *et al* 2011 *Nature Mater.* **10** 521
[29] Bahramy M S, Arita R and Nagaosa N 2011 *Phys. Rev.* B **84** 041202
[30] Eremeev S V *et al* 2012 *Phys. Rev. Lett.* **108** 246802
[31] Crepaldi A *et al* 2012 *Phys. Rev. Lett.* **109** 096803
[32] Landolt G *et al* 2012 *Phys. Rev. Lett.* **109** 116403
[33] Eremeev S V, Nechaev I A and Chulkov E V 2012 *JETP Lett.* **96** 437
[34] Shevelkov A V *et al* 1995 *J. Solid State Chem.* **114** 379
[35] Dönges E 1951 *Z. Anorg. Allg. Chem.* **265** 56
[36] Sakano M *et al* 2013 *Phys. Rev. Lett.* **110** 107204
[37] Lošťák P *et al* 1980 *Phys. Status Solidi* a **59** 311
[38] Rusinov I P *et al* 2013 *Phys. Rev.* B **87** 205103
[39] Kresse G and Hafner J 1993 *Phys. Rev.* B **48** 13115
[40] Kresse G and Furthmüller J 1996 *Comput. Mater. Sci.* **6** 15
[41] Blöchl P E 1994 *Phys. Rev.* B **50** 17953
[42] Kresse G and Joubert D 1999 *Phys. Rev.* B **59** 1758
[43] Perdew J P, Burke L and Ernzerhof M 1995 *Phys. Rev. Lett.* **77** 3865
[44] Koelling D D and Harmon B N 1977 *J. Phys. C: Solid State Phys.* **10** 3107
[45] Gonze X *et al* 2009 *Comput. Phys. Commun.* **180** 2582
[46] Hartwigsen C, Goedecker S and Hutter J 1998 *Phys. Rev.* B **58** 3641